Dual-Tendon Routing: Tendon Routing for Under-Actuated Tendon-Driven Soft Hand-Wearable Robot

Byungchul Kim, *Member, IEEE*, Useok Jeong, and Kyu-Jin Cho, *Member, IEEE*

Abstract—The under-actuated tendon-driven mechanism enables the development of light and compact hand-wearable robots by allowing the robots to assist in adaptive motions. However, tendon friction and elongation accumulate as the tendon passes through many joints, causing hysteresis and detrimental effects on tension distribution, reliability, and efficiency. To mitigate these issues, we present a Dual-Tendon routing (DTR) method and a novel approach to generate $2^{n+1} - 1$ DTRs for robots that actuate n fingers. This letter also introduces five performance factors—adaptability, torsional balance, reliability, efficiency, and transmission ratio—that can be used to find the optimal routings among derived DTRs. The effectiveness of our proposed framework is demonstrated through its application to the Exo-Glove, a soft hand-wearable robot. The reduced friction at the flexion tendon improves under-actuation performance, reduces hysteresis at the flexor, and allows the active extensor to be replaced with a passive tendon. The changed tendon routing also enables the tension sensor to be located at the wearing part in a compact size.

Index Terms—Tendon/wire mechanism, wearable robotics, mechanism design, soft robot applications, rehabilitation robotics.

I. INTRODUCTION

DESIGNING hand-wearable robots necessitates researchers to consider not only the robot's performance in generating firm grasping or dexterous motion but also robot usability, influenced by factors like size, weight, and complexity [1]. Researchers have sought to address these dual demands by integrating soft materials and tendon transmission systems. Soft materials alleviate the need for complex joint alignment mechanisms, while tendon transmissions offer compact, compliant force delivery. The resultant tendon-driven soft hand-wearable robots (TSHRs) offer promising advancements in robotic assistive devices, blending enhanced functionality with user-friendly design [2], [3], [4], [5], [6], [7], [8], [9], [10], [11], [12].

Tendon transmission has the compelling characteristic that it easily actuates serially connected joints. This capability not only improves usability by reducing actuator counts, but also enhances performance by providing adaptability when interacting with the external environment [13]. The adaptive motion increases the number of contact points and, therefore, allows a more stable grasp by enhancing force closure [14]. For this reason, this approach has been widely used in robotic grippers [13], [15], [16], hand-wearable robots [17], [18], and prosthetic hands [19], under the name of an under-actuated tendon routing (UTR). To fully exploit the benefits of UTR, researchers have expanded it to multiple fingers using various design strategies, including movable pulleys (*UTR-M*) [16], fixed pulleys at the end of linkages (*UTR-F*) [17], [18], [20], and specific actuation modules (*UTR-S*) [21], [22].

However, these approaches complicate routings and may cause practical issues. UTR-M, the most common tendon routing for under-actuation mechanism, requires a certain amount of traveling length for the pulleys. Accordingly, to the best of our knowledge, this method has not been used in hand wearable robots as the end-effector size is important in these robots. UTR-F has been proposed as it enables compact wearing part by removing the space for movable pulleys. However, the friction at the fixed pulley was not negligible because URT-F employs conduits (i.e., PTFE tubes) instead of rigid bearings for fixed pulleys due to the size limitation of soft wearable robots [21]. To solve the size and friction issues, researchers have located movable pulleys [21] or differential mechanism [23] at the actuator [UTR-S]. Since the actuator is far from the wearing part, using relatively bulky components (e.g., bearings) was possible. However, this method inherently suffers from tendon elongation caused by the long tendon length because the actuator is located far from the robot. These issues can severely impact robot
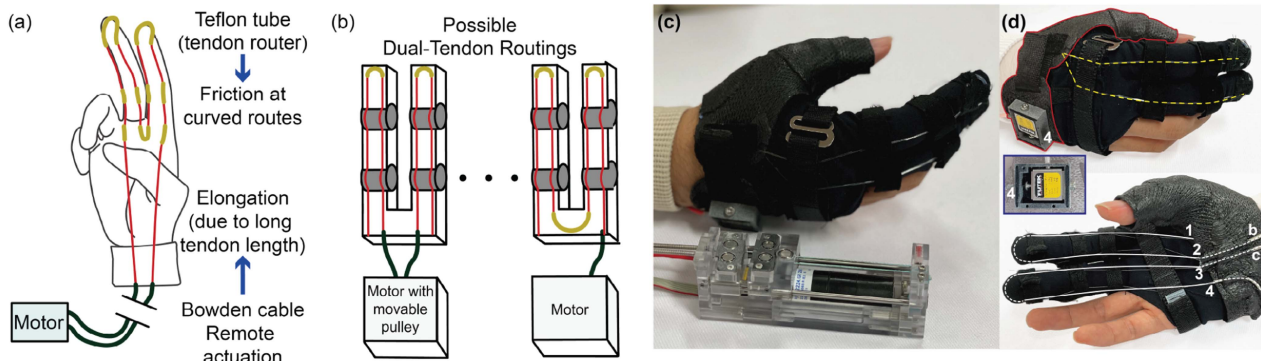
Fig. 1. Overview of the proposed design framework that alleviates the practical issues of the tendon-driven soft wearable robots **(a)** shows the practical issues (friction and elongation at the tendon) in under-actuated soft hand wearable robots. **(b)** shows our strategy to alleviate the practical issues. The strategy finds out the appropriate tendon routing by deriving $2^{(n+1)} - 1$ number of possible dual-tendon routings, an under-actuated tendon routing designed to relieve the practical issue; n is the number of fingers. The researchers can choose proper routing from the obtained routing set according to their requirements. **(c)** shows Exo-Glove II, developed using the tendon routing obtained from our design framework. **(d)** shows the design features of Exo-Glove II. The yellow-dotted line at the top shows the passive extensor of the robot. The region with the red boundary shows the thumb fixation unit; the thumb fixation unit also contains the compact tension sensor (blue rectangle in the middle of the figure). The lower part represents the robot's flexor derived from the proposed design framework.

performance, manifesting as hysteresis, dead zones, compromised observability, and reduced actuation stiffness [24]. Although traditional tendon-driven robots have found ways to mitigate these effects [22], [25], their solutions often rely on rigid components that harm the usability of TSHRs.

These practical issues have significantly impeded progress in under-actuated TSHR design, obstructing other researchers' integration of innovative design ideas. The use of passive extension tendons, previously adopted to simplify robot designs, becomes problematic in systems with high hysteresis. This is because such systems necessitate highly stiff passive tendons, which may lead to unnatural user postures, to overcome high friction at the flexion tendon [17]. Tendon elongation–arising from decreased actuation stiffness–and tendon friction–occurred at the curve of the tendon routing–induce modeling uncertainties. These uncertainties further complicate control strategies, making sophisticated estimation algorithms essential [26], [27]. The dead-zone, caused by the friction, also makes the control complicated [28]. The friction further undermines under-actuation efficiency by leading to uneven tension distribution [21].

In this letter, as shown in Fig. 1, we introduce a *Dual-Tendon routing* (DTR), an under-actuated tendon routing designed to relieve the above issues by integrating UTR-F and UTR-S. This integration leverages the strengths of each routing while mitigating their respective limitations, providing solutions to practical issues. It also enables deriving $2^{n+1} - 1$ number of DTRs for robots that assist n fingers based on the specific combinations of UTR-F and UTR-S. This set of DTR options enables researchers to choose the most appropriate tendon-routing method by evaluating the tension distribution of each configuration. At its core, this framework provides a systematic design process of the DTR, enabling researchers to find the most appropriate tendon routing across various robotic applications.

As a case study, we apply this methodology to the development of Exo-Glove II, an advancement over its predecessor designed to assist individuals with spinal cord injuries [17]. We explore 7 ($2^{(2+1)} - 1$) DTRs and obtain the most appropriate routing for Exo-Glove II by validating them with five performance factors (adaptability, torsional balance, reliability, efficiency, and transmission ratio) by measuring tension distribution of the tendon through the experiments.

Although the proposed framework can be considered as finding the optimal tendon routing, it takes a distinct approach. Prior studies have focused on optimizing specific parameters such as moment arm [29], [30], [31], joint center [32], joint stiffness [30], [33], and the ideal placement of multiple tendons to enhance motion [34]. In contrast, our work explores possible options to route a single tendon across multiple joints and fingers and then select the most appropriate routing from these possibilities. This approach addresses practical challenges, such as friction and elongation, which are significantly influenced by how the tendon passes all joints.

The proposed framework improves the robot as follows: 1) the robot applies more even force to two fingers (the difference in fingertip force is reduced from 19.25% to 9.85%); 2) hysteresis at the flexor is reduced (hysteresis in the joint angle domain is reduced from 63.27% to 27.91%); 3) the tension-sensing unit was installed on the worn part in a compact size, for more accurate tension sensing (compact installation was possible due to the geometrical characteristics of the proposed routing); and 4) the robot wearing part became simpler because the active extensor was replaced with the passive extensor. (it was possible because friction at the flexor was dramatically reduced).

II. METHODS

A. Dual-Tendon Routing

The friction and elongation at the tendon depends on *tendon routing*. Therefore, this research focuses on finding a specific *tendon routing* that minimizes friction and elongation; the expression, *tendon routing* in this letter, represents how both ends of the tendon are connected to the robot and how it passes joints and fingers.

First, we decided to develop our tendon routing on top of the under-actuated tendon routing that only uses fixed pulleys; this routing is named as *soft tendon routing* [17] or *adaptive synergy* [35] previously, but we refer it as *UTRs with fixed-pulleys* (UTR-F) to clearly distinguish with other routings such as UTR-M and UTR-S, not to confuse the readers. We chose this routing as a basis because it has higher actuation stiffness that alleviates the disadvantage of remote actuation [25]. Furthermore, we named the proposed tendon routings as *Dual-Tendon*
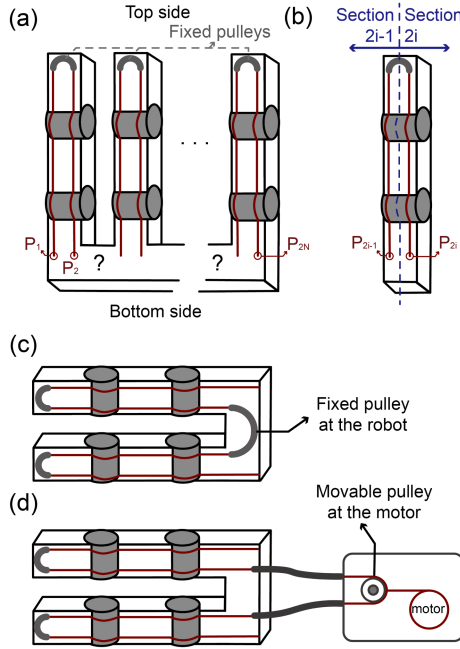
Fig. 2. Schematic of the dual-tendon routings to derive a possible number of dual-tendon routings. **(a)** shows possible methods to route N fingers, with dual-tendon routing. **(b)** shows nominations of the tendon segments and the linkage section at the i-th finger. **(c)** and **(d)** describe two possible routing methods that can be used for the space between the fingers. The fixed pulley in **(c)** is represented as conduits (i.e., PTFE tubes) rather than bearings, as wearable robots utilize conduits to minimize friction at tendon curves due to size constraints.

Routing (DTR) because the tendon passes fingers twice (e.g., section 1 and section 2 in Fig. 3).

The difference between DTR and the UTR-F comes from the diversity of tendon routing methods: the DTR provides $2^{n+1} - 1$ number of designs for n fingers while the UTR-F only provides a single design option when we pull multiple joints with a tendon (single motor). This diversification strategy is possible because DTR design provides two design options at the space between fingers: fixed pulley as shown in Fig. 2(c) or remote movable pulley as shown in Fig. 2(d); it also provides two connection options at the end of the tendon: connecting at the motor or connecting at the robot.

The basic configuration of the DTR for the N linkage system is described in Fig. 2. In DTR, the tendon at the top side of the linkage is routed through the fixed pulley. The tendon at the bottom section, however, can be routed through the fixed-pulley (which is located at the end-effector) or through the movable-pulley (which is located at the actuator side); see Fig. 2(c) and (d). Given the basic configuration of the DTR, possible DTRs are found through the following steps. For the clarity, the tendon points at the bottom side of ith linkage, are referred to as P_{2i-1} and P_{2i} (Fig. 2(b)). Additionally, we assume that the fingers perform only flexion/extension motions, neglecting other directional movements such as abduction/adduction.

First, we considered possible routings at the section between the two linkages (P_2, P_3,..., P_{2N-1}). In this step, 2^{N-1} possibilities can be derived. This is because the tendon between P_{2i-1} and P_{2i} can be routed in two different ways: through the fixed-pulley at the end-effector side (Fig. 2(c)) and through the movable-pulley at the actuator side (Fig. 2(d)).

The second step considers the tendon routing at both ends (P_1 and P_{2N}). In this step, four cases are possible, because both tendon ends can be fixed at the robot or the actuator.

The above two steps provide 2^{N+1} DTRs for the system with N linkages. As a final step, we exclude invalid or overlapping cases. As an invalid case, we consider the situation in which the actuator cannot transmit the tension. When the tendon at P_1 and P_{2N} is fixed at the robot side and the tendon at the other points (P_2, P_3,..., P_{2N-1}) is routed through the fixed-pulley, the robot cannot be actuated because the tendon is not connected to the actuator. We should also consider the overlapping case. When the system has an odd number of linkages, some symmetric cases exist. Accordingly, there exist $2^{N+1} - 1$ DTRs when the system has an even number of linkages and $2^N - 1$ DTRs when the system has an odd number of linkages; if the symmetric cases are considered as different cases, then $2^{N+1} - 1$ DTRs exist, whether the number of linkages is odd or even.

B. Performance Measure of Dual-Tendon Routing

Exo-Glove II is developed by implementing the DTR method to our previous robot called Exo-Glove. Since index and middle finger assistance with passive fixation of the thumb has shown sufficient performance in our previous works [17], [18], Exo-Glove II is also developed to assist two fingers. Accordingly, we can derive seven ($2^{2+1} - 1$) DTRs (which are named TR1 to TR7 in Fig. 3), for our robot. The most suitable routing is chosen by validating them with the five benchmarks proposed in this letter.

The validations use tension at eight segments of a single tendon as shown in Fig. 3; four are on the actuator side (a, b, c, and d) and the other four are on the end-effector side (1, 2, 3, and 4). The tension at each segment is denoted as T_i, where i represents the section label, which can be either 1–4 or a–d. For clarity, the upper finger is referred to as Finger A, with tendon segments 1 and 2, and the lower finger is referred to as Finger B. Based on this segment definition, five performance metrics are obtained by measuring the tension at each section (T_1 to T_4) as outlined in section III-A. This experiment pulled the tendon until the total tension across all sections reached $100N$ (i.e., $\sum_{i=1}^{4} T_i = 100\,\text{N}$).

1) Adaptability Performance: First, we figure out the difference in force applied to the two fingers. This is because the fingertip force differences reduce the grasp stability [17], [18]. The first indicator is defined as

$$\text{I}_{\text{adapt}} = |(T_1 + T_2) - (T_3 + T_4)|. \tag{1}$$

2) Torsional Balance: In soft wearable robots, it is also important to consider unwanted deformations. If there exists a large difference in the tension applied on the finger (i.e., $|T_1 - T_2|$ or $|T_3 - T_4|$), the robot will make unwanted motions such as abduction or adduction motion. Further, this force difference can cause significant failure by applying deformation at the tendon path [12]. We defined the torsional balance performance as the tension difference in the same finger and expressed the corresponding indicator as

$$\text{I}_{\text{tor-bal}} = \max(|T_1 - T_2|, |T_3 - T_4|). \tag{2}$$

3) Reliability: The third indicator measures the reliability of the system. It is defined in terms of friction because the failure is usually caused by the wear in the tendon-driven robot. Since the wear may first appear in the area where the friction is
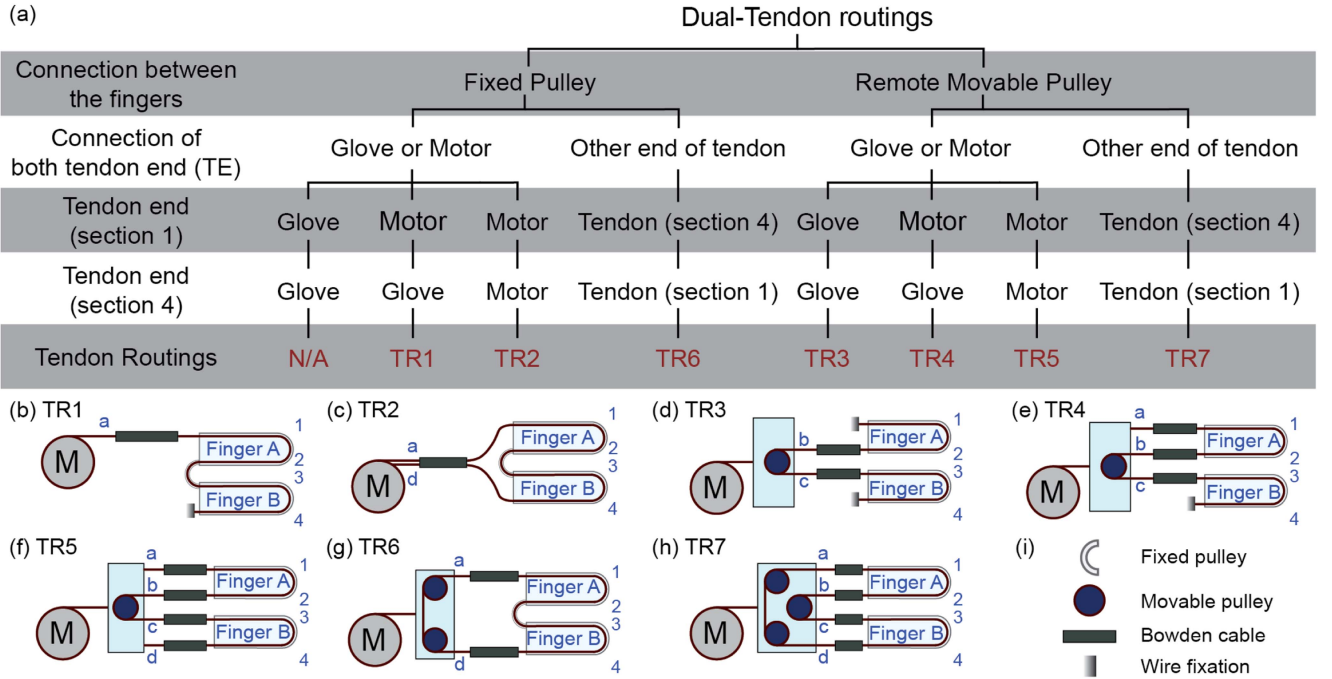
Fig. 3. Derivation of possible dual-tendon routings in the two-linkage system. **(a)** shows the overall view to derive possible dual-tendon routings for two-finger applications. **(b)**–**(h)** show schematics of the dual-tendon routings found for two-finger applications. In these figures, alphabet *a, b, c,* and *d* with blue color mean the tendon section at the motor side; numbers *1, 2, 3,* and *4* with blue color mean the tendon section at the glove side. **(i)** shows a description of the components used in the figure. For example, TR3 shown in **(d)** is the same as the left tendon routing shown in Fig. **1(b)**; TR1 is the same as the right tendon routing in Fig. **1(b)**.

concentrated, the largest frictional force is used for the indicator as

$$I_{\text{reliability}} = \max(f_1, f_2, f_3, \ldots f_n) \quad (3)$$

where f_i means the friction at place i and n means the total number of places where friction occurs at the glove.

4) Efficiency: The fourth indicator is related to the robot's efficiency. It is selected because it affects the size and weight of the actuator and battery. The indicator is expressed as the ratio of the work done by the motor (W_m) and the work done by the end-effector (W_{ee}). The indicator is expressed as

$$I_{\text{efficiency}} = W_{ee}/W_m. \quad (4)$$

5) Force Transmission Ratio: We also consider the last indicator to show the force transmission ratio as

$$I_{\text{transmission}} = (T_1 + T_2 + T_3 + T_4)/T_M \quad (5)$$

where T_M is the summation of tension at the motor side (i.e., $\sum_{i=a}^{d} T_i$). We prefer higher $I_{transmission}$ because it enables researchers to use low-gear ratio motors. The low-gear ratio motor provides back-drivability, low inertia, and torque-sensing capability advantages.

The proposed indicators require normalization because they have different scales. Additionally, the robot's performance is directly proportional to some indicators but inversely proportional to others. Accordingly, we normalize the indicators as

$$N.I_{\text{ad}} = W_A(1 - (|T_1 + T_2 - T_3 - T_4|)/100)$$

$$N.I_{\text{ba}} = W_B(1 - max(|T_1 - T_2|, |T_3 - T_4|)/100)$$

$$N.I_{\text{re}} = W_R(1 - max(f_1, f_2, f_3, \ldots f_n)/100)$$

$$N.I_{\text{ef}} = W_E(W_{finger}/W_{motor})$$

$$N.I_{\text{tr}} = W_T((T_1 + T_2 + T_3 + T_4)/4T_M) \quad (6)$$

where W_A, W_B, W_R, W_E, and W_T represent the weights for the given indicators. The weights are all set to 10 in this letter to make the indicators have a range of 0 to 10.

C. Robot Design

Among 7 tendon routings (Fig. 3(b)–(h)), we developed the Exo-Glove II using TR3 because it showed the best result in the previous validation (Table I). The use of TR3 alleviates the residual friction, as validated in Section III-C, and therefore we could use a passive tendon to extend the finger instead of an active extension tendon, following other previous works; Fig. 1(d) describes the passive extensor as a yellow-dotted line and the active flexor as a white line.

TR3 also provides a qualitative design advantage: it enables the installation of a compact force sensor at the end-effector. This compact installation is possible in TR3 because, both end sides of the tendon can be fixed at the end-effector, as shown in Fig. 3(d). Therefore, we can simply attach the force sensor (as shown in the blue rectangular box in Fig. 1(d)) at the end of the tendon; when we want to measure the tension in the middle of the tendon, we should use a bulkier method similar to that shown in Fig. 4(a). The other end of the tendon, which is not connected to the force sensor, is attached to the thumb fixation unit shown in Fig. 1 because it can sufficiently support reaction force applied by the tension; it not only fixes the thumb but also roles like the *tendon anchoring support* in [17].

TABLE I
PERFORMANCE OF THE DUAL-TENDON ROUTINGS

	$N.I_{ad}$	$N.I_{ba}$	$N.I_{re}$	$N.I_{ef}$	$N.I_{tr}$	Mean
TR1	7.60 (0.145)	9.21 (0.065)	8.88 (0.026)	5.54 (0.072)	5.54 (0.072)	7.35* (0.062)
TR2	9.19 (0.059)	9.52 (0.035)	9.05 (0.011)	6.94 (0.039)	3.47 (0.019)	7.63* (0.015)
TR3	9.96 (0.033)	9.6 (0.046)	9.10 (0.018)	6.95 (0.037)	3.48 (0.019)	**7.82** (0.023)
TR4	6.60 (0.053)	9.48 (0.065)	8.80 (0.020)	7.94 (0.031)	2.65 (0.011)	7.09* (0.027)
TR5	6.37 (0.128)	9.52 (0.134)	8.79 (0.041)	9.31 (0.064)	2.33 (0.016)	7.26* (0.053)
TR6	9.98 (0.046)	9.53 (0.039)	9.09 (0.070)	6.93 (0.089)	3.46 (0.045)	7.80 (0.051)
TR7	9.95 (0.103)	9.83 (0.098)	9.14 (0.119)	7.51 (0.087)	1.88 (0.022)	7.66* (0.073)

Fig. 5.   Tension distribution of possible dual-tendon routings from the proposed design framework. tension distribution of the tendon at the end-effector side. Sections 1 and 2 are sections at finger A; Sections 3 and 4 are sections at finger B in Fig. 3.
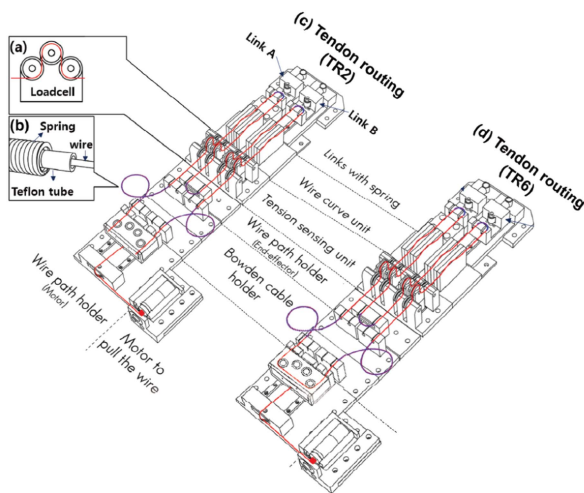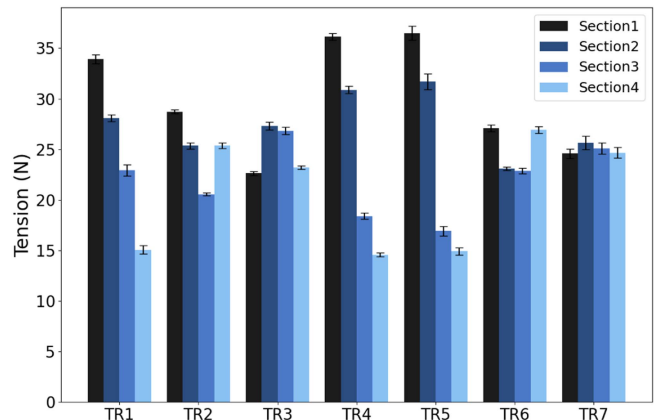

Fig. 4.   Experimental setup to measure the tension distribution of the routings. **(a)** shows the tension-sensing unit and **(b)** shows the detailed structure of the Bowden cable. **(c)** and **(d)** show examples of how the tendon is routed in the actual experiments for experiments TR2 and TR6, respectively. Red lines in the figure represents the tendon. Photos and detailed information of the setup are available on the project website.

III. EXPERIMENTS AND RESULTS

We measured the performance of the Exo-Glove II with obtained tendon routing (TR3) and compared it with that of the robot with the previous tendon routing (TR2). The experiments were conducted using a dummy hand to minimize the influence of unintended voluntary motions.

A. Tension Distribution of Dual-Tendon Routings

The tension distribution of seven DTRs obtained with the experimental setup (Fig. 4) to find the appropriate tendon routing for the Exo-Glove II. Since we are interested in tension at the end-effector part (T_1 - T_4), we installed four load cells (333FB Cell, Ktoyo Co., Ltd., Korea) at the setup (Fig. 4(a)). For the tension of the motor side tendon, we calculated it from the tension at the end-effector side tendon using a friction coefficient at the Bowden cable; it was measured as 0.651 from the other

experiment. For normalized indicators, the experiment is carried out by pulling the tendon using a motor until the sum of the tensions in sections 1 to 4 reaches 100N. The tension distribution of the seven DTRs is in Fig. 5. The normalized indicators of the seven DTRs, calculated from the obtained tension distribution, are shown in Table I.

TR3 demonstrated a significant difference (ANOVA: $p < 0.01$, Mann-Whitney U: $p < 0.01$) from all other DTRs except TR6 (ANOVA: $p = 0.119$, Mann-Whitney U: $p = 0.490$). While we cannot claim that TR3 is better than TR6, TR3 was selected due to its quantitative benefits. Specifically, TR3 allows for a compact load cell installation, as previously described. In contrast, TR6 requires the placement of a fixed pulley between two fingers, which adds complexity to the glove's design. This consideration led us to prefer TR3 for its practicality and simplicity in implementation.

Finding appropriate routing through experiments is not scalable, as the number of required experiments grows exponentially with the number of linkages (fingers). To address this limitation, we have developed a tension distribution model to replace physical experiments. Although there is a sim-to-real gap between the model and experimental results, the closely aligned distribution trends allow us to rely on the modeling as an alternative to conducting experiments. For detailed modeling results, please visit our project website.

B. Adaptability Performance of Dual-Tendon Routing: Fingertip Force Experiment

DTR improves the adaptability (I_{adapt} in (1)). Improved adaptability enhances the grasp stability by applying even force to two fingers [17], [18]. However, directly measuring I_{adapt} is difficult because it is hard to measure the tension at the tendon that passes inside the glove. We alternatively measured the difference in fingertip force between the index and middle finger.

In this experiment, two load-cells (333FB Cell, Ktoyo Co., Korea) were installed at the location where the tip of the index and middle fingers are placed. Fingertip force is measured by pulling the flexor until the sum of two fingertip forces reaches 20 N using the glove with the previous and the proposed tendon routing (TR2 and TR3), respectively, for five times. The
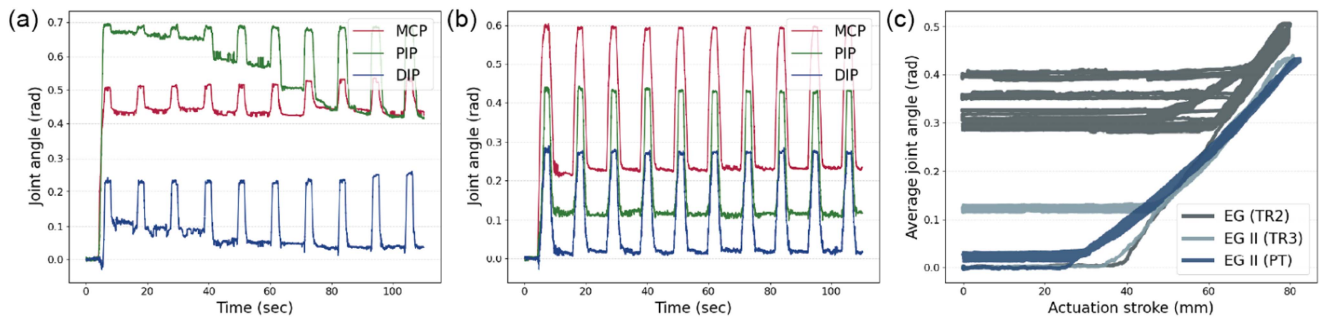
Fig. 6. Hysteresis analysis of the Exo-Glove II. **(a)** shows how the joint moves when the Exo-Glove with the previous routing (TR2) is used; **(b)** shows the joint motion of the robot with the proposed tendon routing (TR3). To enhance readability, the time range is restricted to 0 to 110 seconds in **(a)** and **(b)**, illustrating 10 cycles of joint motion. **(c)** shows the hysteresis at the joint angle represented in the actuation stroke domain; here, the dark gray, gray, and blue graph represent the hysteresis of the Exo-Glove with TR2, the hysteresis of the Exo-Glove II with TR3, and the hysteresis of the Exo-Glove II with TR3 and passive tendons (PT in the legend), respectively.

experimental results show that the differences of force in the previous and proposed robots are measured as 3.85 N and 1.97 N, respectively, with standard deviations of 0.14 and 0.11. Both the ANOVA test (parametric, $p < 0.01$) and the Mann-Whitney U test (non-parametric, $p < 0.01$) confirm a significant difference between TR2 and TR3.

C. Hysteresis Experiment 1: Positional Hysteresis

Since directly measuring the tension at the glove is difficult, similar to the previous case, we conducted two experiments that measure the hysteresis alternatively: 1) an experiment to measure repeated motions to see the positional hysteresis in this subsection and 2) an experiment to measure the force required to extend the finger in the next subsection.

Ideally, due to the elasticity of the finger joints (i.e., joint stiffness or torsional stiffness of spring), the fingers should return to their initial position when the actuators return to their initial position. However, when there exists friction at the tendon, the fingers will return less; we would refer to this phenomenon as *positional hysteresis* in this letter.

To see the positional hysteresis, the joint angles of the index and middle finger were measured with respect to the tendon excursion length. The actuator pulled the flexor 80 mm and released it back to the initial position (0 mm) 20 times, without actuating the extensor. At the same time, the joint angles were measured using six motion-capture cameras (Prime, Optitrack, USA). Ten reflective markers were attached to the fingertip, DIP joint, PIP joint, MCP joint, and at the base of the index/middle fingers, respectively, to calculate the joint angle. Two additional markers were attached to the actuator to measure the actuator displacement, simultaneously. Fig. 6(a) and (b) depict the finger's motion during flexion using the Exo-Glove with the previous tendon routing (TR2) and the proposed tendon routing (TR3), respectively. To visualize the hysteresis that occurs in the two gloves, the average joint angle was also plotted in terms of the actuation stroke, as shown in Fig. 6(c). From this result, we find that the joint angle recovers from 0.49 (0.013) rad to 0.31 (0.035) rad when the previous tendon routing (TR2) is used, while it returns from 0.43 (0.002) rad to 0.12 (0.003) rad with the proposed tendon routing (TR3); the values inside the parentheses indicate standard deviation. For normalization, we also define the 'hysteresis loss' as the ratio between the returned joint angle and the fully flexed joint angle. The hysteresis loss

TABLE II
REQUIRED TENSION TO EXTEND ONE FINGER

	Robot with TR2	Robot with TR3
Extension force after flexion $F_{A.F}$ (N)	5.56 (1.05)	3.85 (0.32)
Extension force without flexion $F_{O.F}$ (N)	2.71 (0.26)	3.05 (0.21)
Normalized indicator $(F_{A.F} - F_{O.F})/F_{O.F}$	1.07 (0.45)	**0.27*** (0.14)

of the previous and the proposed routing are 63.27% (0.31/0.49) and 27.91% (0.12/0.43), respectively. The results of TR2 and TR3 show a significant difference ($P < 0.01$) as confirmed by both the ANOVA test and the Mann-Whitney U test.

D. Hysteresis Experiment 2: Extension Force

We also measured *extension force*, a tension to extend the fingers, to see the hysteresis. When this force is large, we can induce that there exists high friction at the flexor. This is because the extensor should be pulled more strongly to overcome the torque generated by the friction at the flexor.

To measure the extension force, the robots were controlled to fully extend the index/middle fingers. At the same time, tension of the extensor was measured using the loadcell that is located on the actuator side. One thing to note here is that the extension force should be normalized because this indicator is affected by the robot design. For instance, if the extensor moment arm is large, less extension force will be required, even when a large friction remains at the flexor. Since it is challenging to fabricate two robots (i.e., Exo-Glove with TR2 and that with TR3) exactly the same, we normalized the extension force for a more fair comparison.

Therefore, we measured the extension force in two different situations for the normalization. First, the extension force ($F_{A.F}$ in Table II) was measured after making the flexion with the robot. In this measurement, we first flexed the finger and then fully extended the finger using the robot; the actuation force ($F_{A.F}$) was measured in the extension phase, which was done after the flexion phase. Second, we measured the extension force ($F_{O.F}$ in Table II) without including the flexion phase. Here,

the robots fully extended the fingers from their initial position without actuating the flexor.

Ideally, when the friction force at the flexor is zero, the two extension forces should be equal. However, if there is friction force when measuring $F_{A.F}$, the robot should pull the extensor with a larger force compared to the other case. Therefore, we defined the normalized indicator as $(F_{A.F} - F_{O.F})/F_{O.F}$ to represent how much friction at the flexor interferes with the extension motion. The experiments were conducted 20 times to measure $F_{A.F}$ and $F_{O.F}$, with the result described in Table II. The values in parentheses indicate the standard deviation. 400 combinations of $F_{A.F}$ and $F_{O.F}$ were used to calculate the average normalized indicator. The results of TR2 and TR3 show a significant difference, as confirmed by both ANOVA (parametric) and the Mann-Whitney U test (non-parametric) ($p < 0.01$).

E. Effect of Passive Tendon in Hysteresis

In Exo-Glove II, the active extensor is replaced with a passive tendon to simplify the design, as TR3 minimizes hysteresis. To minimize the side effects of using passive tendons, we used a passive tendon with minimal stiffness. Specifically, the passive tendon was chosen to have a stiffness of at least 0.096 N/mm for a displacement of 40 mm, obtained from previous experiment. The proposed robot used a passive tendon with a stiffness of 0.18 N/mm for the final robot, considering the safety factor as 1.9; a tendon-like polyurethane with a diameter of 0.7 mm was used for the passive extensor. To verify whether the passive tendon works effectively, we also conducted the hysteresis experiment again; this experiment was also done under the same experimental condition described in Section III-C.

The results (Fig. 6(c)) show that the average joint angle returns from 0.43 (0.002) rad to 0.02 (0.005) rad when the Exo-Glove with passive tendon assists, where the values inside parentheses mean standard deviation. Comparing this result to previous results, the hysteresis loss of the robot with the passive tendon is only 4.65% (0.02/0.43). From these results, it can be concluded that the Exo-Glove II alleviates the hysteresis by using the passive tendons, while minimizing the side effects (e.g., reduced efficiency, uncomfortable posture, difficulty in wearing) of the passive tendon. This is because the chosen DTR causes less friction at the flexor, allowing the use of a passive tendon with low stiffness.

IV. DISCUSSION & CONCLUSION

Under-actuated tendon-driven soft wearable robots often experience uneven tension distribution and large friction at the tendon. Finding the optimal tendon routing to minimize these effects is challenging, as tension distribution is heavily influenced by how the tendon passes joints. Moreover, routings that pass through many joints and fingers are not unique, necessitating the exploration of all possible routing configurations by researchers.

This letter proposes a framework that solves these issues by systematically deriving $2^{n+1} - 1$ dual-tendon routings, under-actuated tendon routings proposed in this letter by combining UTR-F that uses fixed pulleys and UTR-S that uses specific actuators, for the n fingers application. With five indicators proposed in this letter, the most appropriate routing for given application is obtained. The next version of the Exo-Glove, designed with the selected DTR, is presented, and its performance is compared

with that of the robot utilizing the previous routing in Sections III-B–III-E.

Although tendon routings other than TR3 were not applied in Exo-Glove II, this framework provides intuition to design routings for other applications with different requirements. TR1, a tendon routing that uses three fixed pulleys, shows relatively low performance because friction is accumulated as the tendon passes the joints and fingers. However, it generates a high force compared to other tendon routings because it has the biggest I_{tr}. Therefore TR1 can be used where a large grasping force is required with a small actuation force. For example, GRIPIT, a hand-wearable device that assists with the tripod grasp, can be a good example for this routing [36]; it required sufficient force even with a small tension because the device was designed to be pulled manually. Therefore, the routing similar to TR1 worked great for this application.

When different amounts of tension should be applied on different fingers, TR4 and 5 can be useful. Here, the tension applied on the two fingers shows a big difference because the tendon moves from one finger to the other finger through the Bowden cable. Due to this characteristic, they can make a sequential motion, similar to the Pisa/IIT Soft hand II [20]. For instance, they can be used to make a lateral pinch grasp; in this posture, high force is applied to the thumb, while the force applied to the other fingers remains small.

The tendon routing similar to TR2 can be used for a case that requires locating the actuator at the end-effector. This is because TR1 and TR2 do not require any movable pulleys; therefore, it is possible to locate a small-sized actuator (e.g., slack-enabling actuator) at the end-effector.

The proposed framework offers four key advantages. First, it serves as a guideline for designing under-actuated tendon-driven robots, enabling researchers to systematically design tendon routings by providing whole possible routings instead of relying solely on intuition. Second, the proposed routing allows the robot to assist with a more stable grasp by reducing the difference in the fingertip forces. Third, the hysteresis at the flexor is dramatically reduced; therefore, the robot can control the motion more accurately. The decrease of hysteresis also reduces the tension required to extend the finger, allowing more stable operation. Thanks to this advantage, it was possible to reduce the robot's complexity by replacing the extensor with a passive tendon. Lastly, it allows the tension-sensing unit to be attached to the wearing part in a compact size; therefore, it was possible to control the tension at the end-effector more accurately.

One limitation of the framework is that it only finds the possible tendon routings. Therefore, in future work, we should consider the framework that optimizes design parameters to further develop the robots. For instance, joint torque highly depends on the moment arm of the tendon. Therefore, we cannot figure out the exact motion or force with this framework. Accordingly, we will integrate the proposed framework with the optimization framework.

We expect that the proposed framework can provide a good guideline for designing the tendon routing. This is because this framework provides all possible tendon routings for a given robot system, unlike other optimization frameworks [32], [33], [34], which find a single tendon routing that minimizes the cost function. Therefore, we expect that researchers will be able to develop tendon-driven robots using the proposed framework, considering other qualitative factors (e.g., tendon routing that can install the tension sensor in a compact size, as described

in this letter) that are important for the specific robot and its application.

REFERENCES

[1] T. Bützer, O. Lambercy, J. Arata, and R. Gassert, "Fully wearable actuated soft exoskeleton for grasping assistance in everyday activities," *Soft Robot.*, vol. 8, no. 2, pp. 128–143, 2021.

[2] S. W. Lee, K. A. Landers, and H. S. Park, "Development of a biomimetic hand exotendon device (BiomHED) for restoration of functional hand movement post-stroke," *IEEE Trans. Neural Syst. Rehabil. Eng.*, vol. 22, no. 4, pp. 886–898, Jul. 2014.

[3] B. Kim, J. Ryu, and K.-J. Cho, "Joint angle estimation of a tendon-driven soft wearable robot through a tension and stroke measurement," *Sensors (Switzerland)*, vol. 20, no. 10, 2020, Art. no. 2852.

[4] D. H. Kim and H. S. Park, "Cable actuated dexterous (CADEX) glove for effective rehabilitation of the hand for patients with neurological diseases," in *Proc. IEEE Int. Conf. Intell. Robots Syst.*, 2018, pp. 2305–2310.

[5] W. Chen et al., "Soft exoskeleton with fully actuated thumb movements for grasping assistance," *IEEE Trans. Robot.*, vol. 38, no. 4, pp. 2194–2207, Aug. 2022.

[6] S. W. Lee, K. A. Landers, and H.-S. Park, "Development of a biomimetic hand exotendon device (biomHED) for restoration of functional hand movement post-stroke," *IEEE Trans. Neural Syst. Rehabil. Eng.*, vol. 22, no. 4, pp. 886–898, Jul. 2014.

[7] L. Gerez, A. Dwivedi, and M. Liarokapis, "A hybrid, soft exoskeleton glove equipped with a telescopic extra thumb and abduction capabilities," in *Proc. 2020 IEEE Int. Conf. Robot. Automat.*, 2020, pp. 9100–9106.

[8] R. Alicea, M. Xiloyannis, D. Chiaradia, M. Barsotti, A. Frisoli, and L. Masia, "A soft, synergy-based robotic glove for grasping assistance," *Wearable Technol.*, vol. 2, 2021, Art. no. e4.

[9] D. H. Kim, Y. Lee, and H.-S. Park, "Bioinspired high-degrees of freedom soft robotic glove for restoring versatile and comfortable manipulation," *Soft Robot.*, vol. 9, no. 4, pp. 734–744, 2022.

[10] T. Bagneschi, D. Chiaradia, G. Righi, G. Del Popolo, A. Frisoli, and D. Leonardis, "A soft hand exoskeleton with a novel tendon layout to improve stable wearing in grasping assistance," *IEEE Trans. Haptics*, vol. 16, no. 2, pp. 311–321, Apr.–Jun. 2023.

[11] A. Yurkewich, I. J. Kozak, D. Hebert, R. H. Wang, and A. Mihailidis, "Hand extension robot orthosis (HERO) grip glove: Enabling independence amongst persons with severe hand impairments after stroke," *J. Neuroeng. Rehabil.*, vol. 17, 2020, Art. no. 33.

[12] B. Kim, H. Choi, K. Kim, S. Jeong, and K.-J. Cho, "Exo-Glove Shell: A hybrid rigid-soft wearable robot for thumb opposition with an under-actuated tendon-driven system," *Soft Robot.*, vol. 12, pp. 22–33, 2024.

[13] J. Yi, B. Kim, K.-J. Cho, and Y.-L. Park, "Underactuated robotic gripper with fiber-optic force sensing tendons," *IEEE Robot. Automat. Lett.*, vol. 8, no. 11, pp. 7607–7614, Nov. 2023.

[14] L. Birglen and C. M. Gosselin, "Force analysis of connected differential mechanisms: Application to grasping," *Int. J. Robot. Res.*, vol. 25, no. 10, pp. 1033–1046, 2006.

[15] G. Xie, L. Chin, B. Kim, R. Holladay, and D. Rus, "Strong compliant grasps using a cable-driven soft gripper," in *Proc. 2024 IEEE/RSJ Int. Conf. Intell. Robots Syst.*, 2024, pp. 8696–8703.

[16] A. M. Dollar and R. D. Howe, "The highly adaptive SDM hand: Design and performance evaluation," *Int. J. Robot. Res.*, vol. 29, no. 5, pp. 585–597, 2010.

[17] H. In, B. B. Kang, M. Sin, and K.-J. Cho, "Exo-Glove: A wearable robot for the hand with a soft tendon routing system," *IEEE Robot. Automat. Mag.*, vol. 22, no. 1, pp. 97–105, Mar. 2015.

[18] B. B. Kang, H. Choi, H. Lee, and K.-J. Cho, "Exo-Glove Poly II: A polymer-based soft wearable robot for the hand with a tendon-driven actuation system," *Soft Robot.*, vol. 6, no. 2, pp. 214–227, 2019.

[19] T. Lalibert, G. Cl'ement, and F. Pelletier, "An anthropomorphic underactuated robotic hand with 15 dofs and a single actuator," in *Proc. IEEE Int. Conf. Robot. Autom.*, 2008, pp. 749–754.

[20] C. D. Santina, C. Piazza, G. Grioli, M. G. Catalano, and A. Bicchi, "Toward dexterous manipulation with augmented adaptive synergies: The Pisa/IIT softhand 2," *IEEE Trans. Robot.*, vol. 34, no. 5, pp. 1141–1156, Oct. 2018.

[21] B. Kim, U. Jeong, B. B. Kang, and K.-J. Cho, "Slider-tendon linear actuator with under-actuation and fast-connection for soft wearable robots," *IEEE/ASME Trans. Mechatron.*, vol. 26, no. 6, pp. 2932–2943, Dec. 2021.

[22] G. Palli and C. Melchiorri, "Friction compensation techniques for tendon-driven robotic hands," *Mechatronics*, vol. 24, no. 2, pp. 108–117, 2014. [Online]. Available: https://www.sciencedirect.com/science/article/pii/S0957415813002407

[23] L. Gerez, J. Chen, and M. Liarokapis, "On the development of adaptive, tendon-driven, wearable exo-gloves for grasping capabilities enhancement," *IEEE Robot. Automat. Lett.*, vol. 4, no. 2, pp. 422–429, Apr. 2019.

[24] D.-H. Lee, Y.-H. Kim, J. Collins, A. Kapoor, D.-S. Kwon, and T. Mansi, "Non-linear hysteresis compensation of a tendon-sheath-driven robotic manipulator using motor current," *IEEE Robot. Automat. Lett.*, vol. 6, no. 2, pp. 1224–1231, Apr. 2021.

[25] Y. J. Kim, "Anthropomorphic low-inertia high-stiffness manipulator for high-speed safe interaction," *IEEE Trans. Robot.*, vol. 33, no. 6, pp. 1358–1374, Dec. 2017.

[26] T. Do, T. Tjahjowidodo, M. Lau, and S. J. Phee, "Nonlinear friction modelling and compensation control of hysteresis phenomena for a pair of tendon-sheath actuated surgical robots," *Mech. Syst. Signal Process.*, vol. 60-61, pp. 770–784, 2015. [Online]. Available: https://www.sciencedirect.com/science/article/pii/S0888327015000035

[27] Z. Sun, Z. Wang, and S. J. Phee, "Elongation modeling and compensation for the flexible tendon–sheath system," *IEEE/ASME Trans. Mechatron.*, vol. 19, no. 4, pp. 1243–1250, Aug. 2014.

[28] X. Liu, W. Jiang, and X.-C. Dong, "Nonlinear adaptive control for dynamic and dead-zone uncertainties in robotic systems," *Int. J. Control, Automat. Syst.*, vol. 15, no. 2, pp. 875–882, 2017.

[29] H. Dong, E. Asadi, C. Qiu, J. Dai, and I.-M. Chen, "Geometric design optimization of an under-actuated tendon-driven robotic gripper," *Robot. Comput.- Integr. Manuf.*, vol. 50, pp. 80–89, 2018.

[30] T. Chen, L. Wang, M. Haas-Heger, and M. Ciocarlie, "Underactuation design for tendon-driven hands via optimization of mechanically realizable manifolds in posture and torque spaces," *IEEE Trans. Robot.*, vol. 36, no. 3, pp. 708–723, Jun. 2020.

[31] H. Basumatary and S. M. Hazarika, "Design optimization of an under-actuated tendon-driven anthropomorphic hand based on grasp quality measures," *Robotica*, vol. 40, no. 11, pp. 4056–4075, 2022.

[32] J. M. Inouye and F. J. Valero-Cuevas, "Anthropomorphic tendon-driven robotic hands can exceed human grasping capabilities following optimization," *Int. J. Robot. Res.*, vol. 33, no. 5, pp. 694–705, 2014.

[33] M. Kim, J. Park, J. Kim, and M. Kim, "Stiffness decomposition and design optimization of under-actuated tendon-driven robotic systems," in *Proc. 2018 IEEE Int. Conf. Robot. Automat.*, 2018, pp. 2266–2272.

[34] D. Bauer et al., "Design and control of foam hands for dexterous manipulation," *Int. J. Humanoid Robot.*, vol. 17, no. 01, 2020, Art. no. 1950033.

[35] M. G. Catalano, G. Grioli, E. Farnioli, A. Serio, C. Piazza, and A. Bicchi, "Adaptive synergies for the design and control of the Pisa/IIT SoftHand," *Int. J. Robot. Res.*, vol. 33, no. 5, pp. 768–782, 2014.

[36] B. Kim, H. In, D.-Y. Lee, and K.-J. Cho, "Development and assessment of a hand assist device: GRIPIT," *J. NeuroEng. Rehabil.*, vol. 14, no. 1, 2017, Art. no. 15.